Total recycling of low-quality urban-fringe construction and demolition waste towards the development of sustainable non-cement pervious concrete: The proof of concept

Qiang Zeng[a,*], Nidu Jike[a], Yu Peng[a], Jiyang Wang[a], Mingzhong Zhang[b], Yuxi Zhao[a]

[a] *College of Civil Engineering and Architecture, Zhejiang University, 310058, Hangzhou, P.R. China*
[b] *Department of Civil, Environmental and Geomatic Engineering, University College London, London, WC1E 6BT, UK*

Abstract

This work provided a proof-of-concept study of recycling low-quality urban-fringe construction and demolition waste (CDW) for the development of sustainable non-cement pervious concrete. CDW in-situ collected from a local construction site of urban-fringe in Hangzhou, China, was elaborately analyzed for quality assessment. Ground brick powder was activated by alkali activators (NaOH and Na_2SiO_4) to fabricate the binding material, and the optimal mixing ratio was investigated. Macro CDW solids and alkali-activated recycled brick powder (AARBP) were used as the aggregate and binding material, respectively, to achieve the CDW's total recycling. The effects of binder-to-aggregate ratio on the engineering performances and multi-scale structures of the non-cement recycled CDW pervious concrete were explored. Results showed that the AARBP paste had the strength up to 50 MPa at the Al+Si/Na (AS/N) ratio of 6.3. The non-cement recycled CDW previous concrete showed relatively low compressive strength but high water permeability. Microstructural mechanisms in the aspects of pores, skeletons, and matrix-aggregate interactions were explored. The findings of this

*Corresponding author
Email address: cengq14@zju.edu.cn (Qiang Zeng)

work provide a promising route towards solving the large-scale CDW in China.

Keywords: Recycling; Pervious concrete; Strength; Microstructure.

1. Introduction

The continual urbanization currently occurring in China triggers the large-scale constructions of infrastructures and buildings, which, however, simultaneously produce massive construction and demolition waste (CDW) that increases the landfill, and pollutes the air and water in local cites (Li et al., 2020c). The rapid annual increment of CDW and the low recycling rate (around 5%) in China jointly put high economic and environmental stresses (Duan et al., 2019). It was estimated that the annual accumulation of CDW was raised up to over 2.4 billion tones (Yazdani et al., 2021), and around three-quarter of Chinese cities suffered excessive CDW (Ma et al., 2020). While policies issued by Chinese government attempt to encourage the reuse and recycling of CDW, the recycling efficiency of CDW faces difficulties due to different reasons, such as, the huge variances in CDW source and quality, and the lack of tracing system of resources, products and wastes (Ma et al., 2020). Challenges rise for the high efficient uses of low-quality CDW that doesn't meet the requirements of engineering applications.

At present, a common way of CDW recycling is to reuse the inert phases of CDW with relatively high mechanical properties and volume stability (e.g., concrete, brick, ceramic and mortar) after complete or partial processes of screening, crushing, sieving, separating and washing. Generally, those inert wastes can be directly used as secondary construction material to totally or partially replace natural aggregate and/or filler in the engineering scenarios of pavement subgrade (Zhang et al., 2021), and recycled aggregate for concrete construction (Robalo et al., 2021; Olofinnade and Ogara, 2021). Xiao and coworkers have systematically investigated the engineering properties of concrete with CDW aggregate and filler (Duan et al., 2020a,b; Sun et al., 2021). Moreover, CDW may act as the source materials for geopolymer fabrication (Ulugol et al., 2021a,b), composite manufacturing (Sormunen and Karki, 2019; Clark et al., 2020), and functional materials development for control of environmental noise (Amarilla et al., 2021).

Compared with natural aggregate, recycled CDW aggregate often possesses lower crushing index, but higher water absorption due to the existence of porous phases like recycled mortar and brick. Therefore, the direct substitution of natural aggregate by recycled CDW aggregate for concrete manufacture generally causes the substantial decrease of workability, strength and permeability resistance (Duan et al., 2020a; Olofinnade and Ogara, 2021; Meng et al., 2021). For example, Liu et al. (2020) evidenced the negatively effects of recycled brick particles with low material strength, rough particle surfaces, and high porous microstructure on the workability and strength of concrete and mortar. Strengthening techniques were therefore developed for the proper uses of CDW in construction materials manufactures. Xiao et al. (2018) reported that the milling of CDW to powder (named mechanical activation) can retain the mechanical properties of concrete with CDW powder ratio up to 45%. Meng et al. (2021) suggested that, compared with the concrete blended with untreated CDW, the activation of CDW with nano particles can substantially increase the mechanical properties of concrete with the same CDW replacement ratio.

Alternatively, it would be a proper solution to avoid the low engineering properties of CDW for developing construction materials with relatively low strength and permeability thresholds like pervious concrete. The uses of pervious materials in pavements, roads, parking lots and riverbanks raised by the development of sponge cities (Shen et al., 2020) would bring the additional benefits to mitigate the urban heat-island effect (Chen et al., 2019; Liu et al., 2020; Tan et al., 2021) and waterlog disaster (Cai et al., 2018; Zhou et al., 2021). Great efforts therefore have been made to develop pervious concrete with high content of CDW as the aggregate (Ibrahim et al., 2020; Debnath and Sarkar, 2020; Lu et al., 2019; Vieira et al., 2020). However, ordinary Portland cement (OPC) is generally used as the binding material in most CDW pervious concretes, which, is blamed for the high energy consumption and CO_2 emissions of cement production (IEA, 2020). Therefore, it provides strong incentives to develop new eco-friendly cementitious material to replace OPC for CDW pervious concrete manufacture. Alkali activation may be a preferable technique to develop low-carbon binder, as part of the silica and alumina in CDW inerts like sintered clay brick, ceramics and glasses show active potentials (Li et al., 2020a,b; Collivignarelli et al., 2021; Ulugol et al., 2021a,b). For instance, alkali-activated CDW was used to construct road sudgrade (Bassani et al., 2019a,b; Tefa et al., 2021) and masonry unit (Zhang et al., 2021). Inspired by the high sustainability of alkali-activated CDW binder, great significance will rise for pervious concrete manufactured by both CDW binder and aggregate, which may be termed as non-cement pervious concrete with total CDW recycling.

The main goal of this work is developing a feasible technique for the total recycling of low-quality CDW for non-cement pervious concrete manufacture. To this end, alkali-activated recycled brick powder (AARBP) alternative to cement was used as binder to replace OPC on one hand, a low-quality CDW was recycled as aggregate on the other hand. The low-quality CDW used in this work was in-situ collected from a local urban-fringe of Hangzhou, China, and their physical properties were comprehensively characterized. Specific experimental schemes were designed to 1) optimize the mix proportions of AARBP paste, and 2) fabricate non-cement CDW pervious concrete. Structures of pores, skeletons and matrix-aggregate interfacial transition zones (ITZs) were characterized by X-ray computed tomography (XCT) and scanning electron microscopy (SEM). Profound discussions were performed to explore the microstructural mechanisms of engineering performances of the non-cement CDW pervious concrete. The technique developed in this work may broaden the ways to relax the environmental stresses raised by the massive pileup of CDW and CO_2 emissions by cement uses.

2. Characterization of low-quality CDW

The ongoing constructions and demolitions in local urban-fringe of Hangzhou, China, stimulated by the 2022 Asian Games simultaneously raised new buildings and piled up massive CDW. As an example, Fig. 1a shows the mountainous pile of CDW in a construction site, Gongshu district of Hangzhou, Zhejiang. A recycling factory (Hangzhou Qianjiangxincheng Municipal Garden Construction Co., Ltd) has been established near the construction site for coarse materials recycling. CDW was crushed, sieved and partially recycled, where the inerts with particle size between 10 and 45 mm were recycled

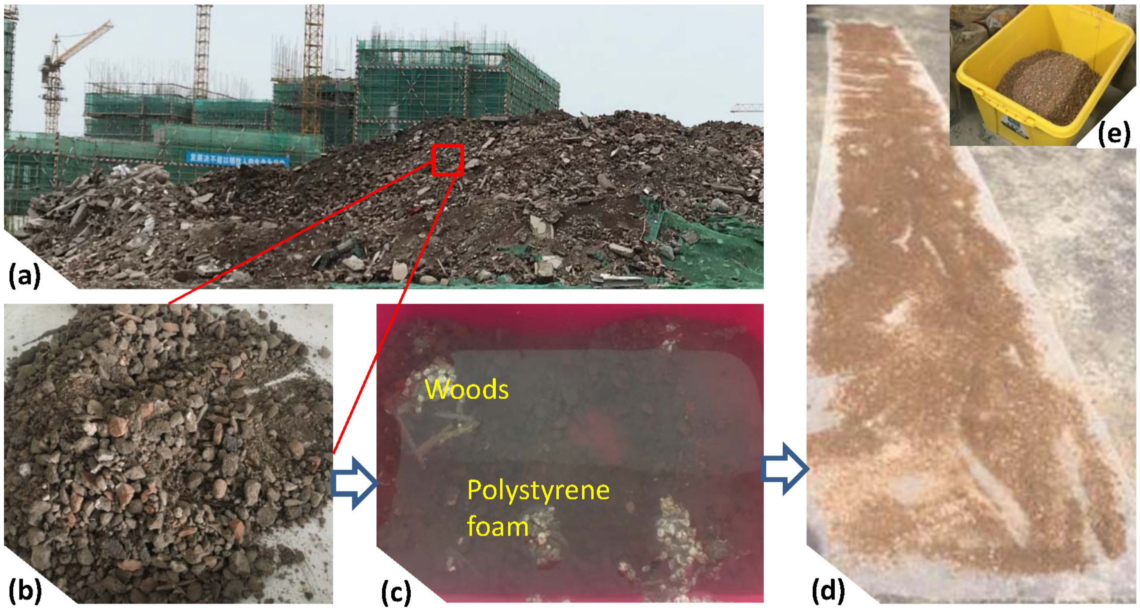

Figure 1: (a) Pileup of CDW in a local area of Hangzhou (Zhejiang province, China. Photographed by the corresponding author at 16, July, 2020), (b) low-quality CDW after crushing and sieving, (c) washing of the CDW to remove the light woods and plastics, (d) drying of the CDW in the sun, (e) storage of the CDW solids in a box.

as aggregate after washing, but the rest can not be directly recycled due to complex compounds and poor properties. Therefore, the untreated CDW particles with size below 10 mm may be classified as a type of low-quality CDW (Fig. 1b). Large scale of low-quality CDW that pileups everyday raises stresses on land circulation of Hangzhou.

The obtained low-quality CDW, a mixture of different compounds, was first immersed in water to distinguish between light materials (e.g., wood and foam plastics) and sediments (Fig. 1c). The light materials were removed, while the rest sediments were retained for further processes. After an air-drying process by sunlight exposure (Fig. 1d), the sediments were stored in a box for further tests (Fig. 1e).

The dried low-quality CDW was then sieved in a sieving system to analyze particle size distribution (PSD) (Fig. 2a). Particles in the size ranges of below 1.18 mm, 1.18-2.36 mm, 2.36-4.75 mm, 4.75-9.5 mm and over 9.5 mm occupied 22.4%, 18.%, 21.3%, 32.3% and 6.6% of the total low-quality CDW by mass (Fig. 2b). Typical morphology of those particles at different size levels is shown in Fig. 2c. It is noteworthy that the CDW with size below 1.18 mm can be sorted as dusts and soils, which thus can not directly recycled as the fillers for construction materials. Therefore, the waste particles with size over 1.18 mm were retained and recycled as the aggregate for further engineering applications.

Component analysis was further performed on the cleaned and sieved CDW sample (particle size over 1.18 mm). Fig. 3a-i demonstrates typical pictures of the main phases classified from 1 kg low-quality CDW inert. Crushed concrete pieces (aggregates covered with cement mortar), clean stones, and bricks took the most mass fractions (i.e., 59%wt, 26%wt, and 10%wt, respectively), while the remainders , i.e., ceramic, glass, wood, slag, gypsum and metal, only occupied the rest 5%wt (Fig. 3j). The ceramic, glass, wood and gypsum may come from decoration materials in the urban-fringe building demolitions. Nails in different specifications were observed (Fig. 3i). Component complexity of the low-quality CDW increased recycling difficulties.

The sieved CDW aggregates then experienced the tests of engineering properties. The obtained bulk density, crushing index and water absorption were 1350 kg/m^3, 15.9% and 8.5% . According to a Chinese standard (GB/T 25177-2010), the CDW inert cannot be directly recycled as the aggregate for construction concrete production,

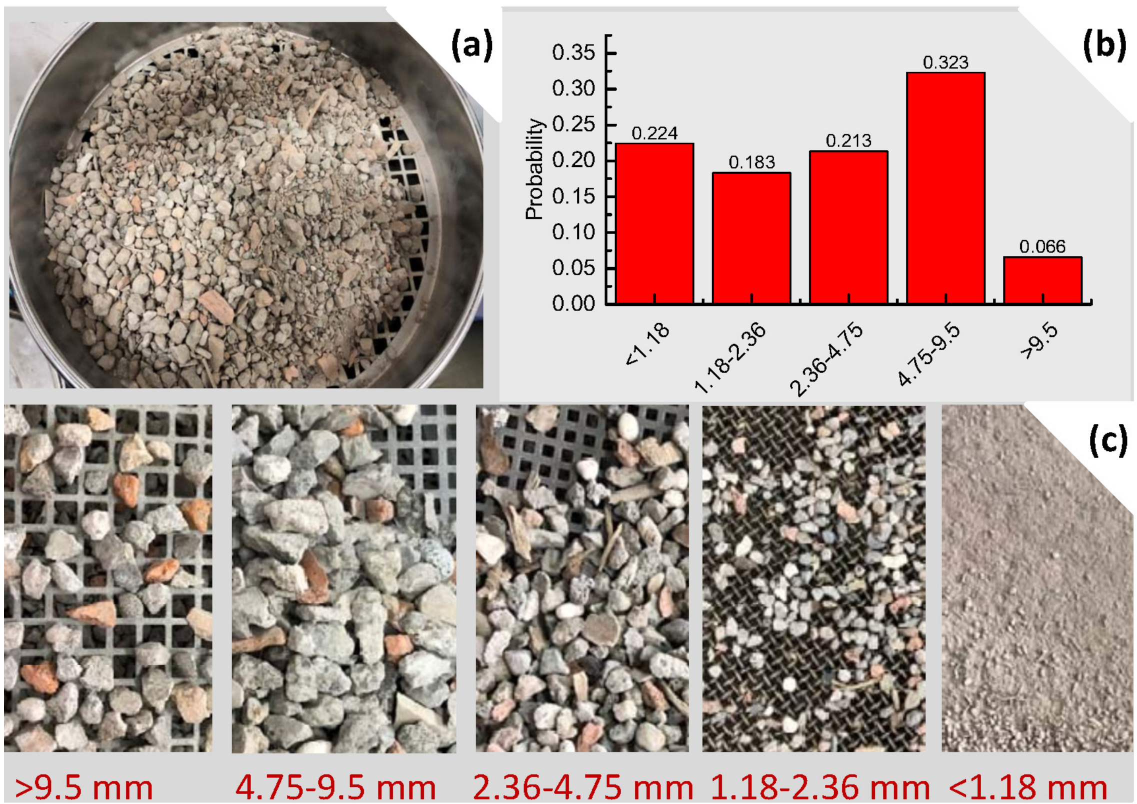

Figure 2: (a) Sieving of the cleaned and dried CDW, (b) particle size distribution of the CDW, (c) pictures of the sieving residue of different size ranges.

Figure 3: Classification of the CDW sample with size over 1.18 mm: (a) recycled concrete, (b) stone, (c) brick, (d) ceramics, (e) glass, (f) wood, (g) slag, (h) gypsum, (i) metals, and (j) their mass percentages.

because the water absorption was higher than the threshold index (<8%). Therefore, new techniques to use those low-quality CDW should be developed.

3. Experiments and methods

3.1. Experimental design

In this work, in addition to the ordinary recycling of CDW as aggregate, the alkali activation technique was applied to activate brick powder as the binding material alternative to cement for achieving the maximum sustainability (Bassani et al., 2019a,b; Tefa et al., 2021; Collivignarelli et al., 2021; Ulugol et al., 2021a,b). The sketch of experimental design is displayed in Fig. 4. The experimental work consisted of two main parts.

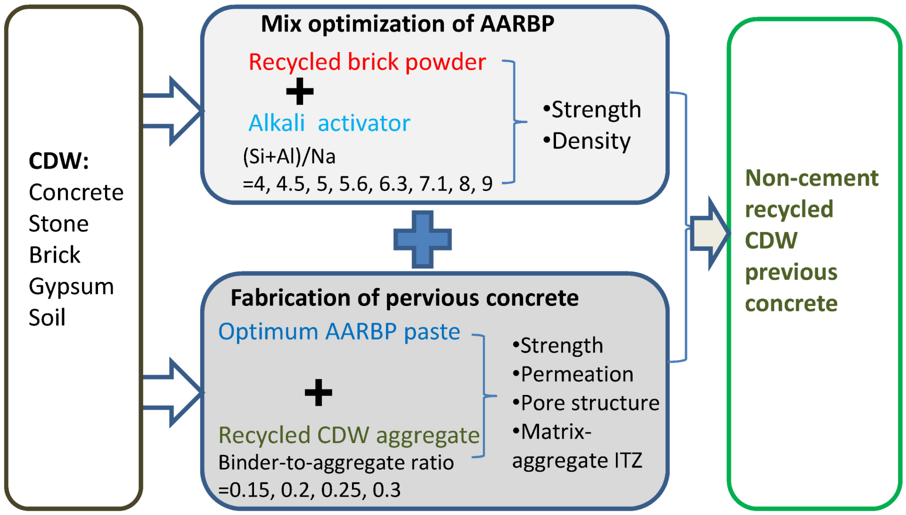

Figure 4: Experimental scheme for the development of non-cement recycled CDW previous concrete.

- Optimization of AARBP mixes. Finding out the appropriate mix proportions between the brick powder and alkali activators was the premise to use AARBP as the binding material. Different molar ratios of $(Al_2O_3 + SiO_2)/Na_2O$ (abbreviated as AS/N ratios) were designed according to (Reig et al., 2013; Robayo et al., 2016; Tuyan et al., 2018). Mix optimization was performed based on strength data (Fig. 4).

- Fabrication of non-cement CDW pervious concrete. The optimum AARBP mix was adopted to prepare the paste that acts as the binding material to bond together the low-quality CDW aggregates. Because the content of binding material can greatly impact the properties of pervious concrete, four different binder-to-aggregate (B/A) ratios were designed (B/A=0.15, 0.2, 0.25, and 0.3 by mass). The properties of compressive strength and water permeability coefficient were tested, and the material features of pore structure, skeleton and matrix-aggregate

ITZ were characterized with multi-scale tests (Fig. 4).

3.2. Sample preparation

3.2.1. Preparation of AARBP

Waste sintered clay bricks were collected from the same demolitions, and crushed into macro pieces by a jaw crushing machine (Fig. 5a). The macro brick pieces were then ground to powder by a ball milling machine for 2 h (Fig. 5b). PSD of the brick powder was tested via a laser particle size analyzer (Beckman Coulter LS 230). The most probably particle size at the peak of differential PSD curve was 60.3 μm, and D50 was 30.2 μm (Fig. 5c). The brick powder showed the similar fineness to a type of recycled brick dust (Li et al., 2020d), but coarser than some highly milled brick powders (Tang et al., 2020) and Portland cement (Li et al., 2020b).

X-ray fluorescence (XRF) test was performed to measure the main oxides in the recycled brick powder. Silica, alumina and ferric oxide occupied the ulmost mass of the brick sample (over 92%wt), while potassium oxide, magnesium oxide and calcium oxide occupied 6.4%wt and other oxides were all less than 0.5% (Fig. 5d). Similar chemical component distribution was reported for other recycled bricks and ceramics (Tuyan et al., 2018; Liu et al., 2020; Li et al., 2020a).

The chemical mechanisms of using brick powder as the binding material are that part of the silica and alumina in the sintered clay bricks would show potential chemical activities under highly alkaline environments (Tuyan et al., 2018; Bassani et al., 2019a,b; Tefa et al., 2021; Ulugol et al., 2021a,b). Here sodium silicate solution (Na_2SiO_4 with

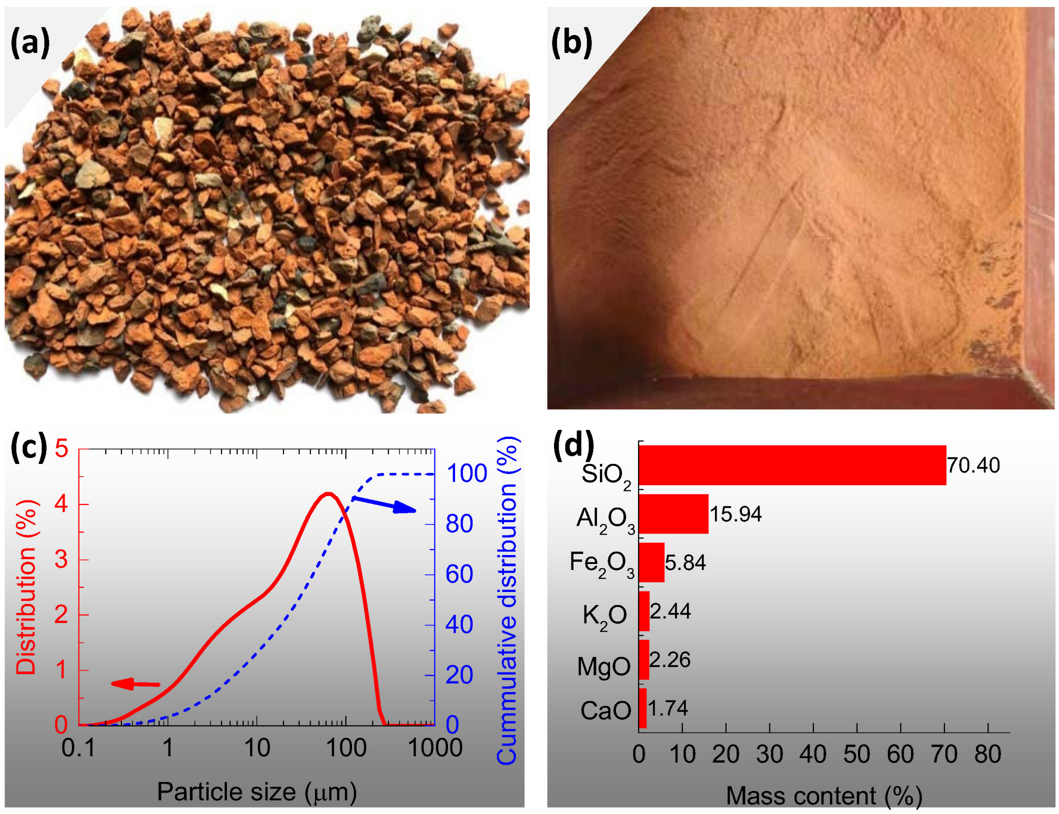

Figure 5: (a) Crushed brick particles and (b) brick powder after ball milling, (c) PSD of the brick powder, and (d) the main oxides in the brick powder tested by XRF.

SiO_2 = 27.35%, Na_2O = 8.42%, and H_2O = 64.23%) and sodium hydroxide ($Na(OH)_2$ with Na_2O = 77.4%, and H_2O = 22.5%, impurity =0.1%) were used as the activators. Both the sodium silicate solution and sodium hydroxide were purchased from Sinopharm Chemical Reagent Co., Ltd. The sodium silicate solution, sodium hydroxide and solvent water were first mixed to prepare the alkali activator solutions. The solutions first settled for 4 hours before mixing to eliminate the solutions' instability (Yan et al., 2016).

Table 1: Mix proportions of AARBP paste

Sample ID	Brick powder (g)	Na_2SiO_4 (g)	NaOH (g)	AS/N ratio	W/B ratio
BP-AS/N-4.0	1000	456	120.03	4.0	0.3
BP-AS/N-4.5	1000	456	101.72	4.5	0.3
BP-AS/N-5.0	1000	456	85.56	5.0	0.3
BP-AS/N-5.6	1000	456	71.20	5.6	0.3
BP-AS/N-6.3	1000	456	58.35	6.3	0.3
BP-AS/N-7.1	1000	456	46.78	7.1	0.3
BP-AS/N-8.0	1000	456	36.32	8.0	0.3
BP-AS/N-9.0	1000	456	26.81	9.0	0.3

The AS/N ratios of 4, 4.5, 5, 5.6, 6.3, 7.1, 8, and 9 were designed to screen the optimum mixes under a constant water-to-binder (W/B) ratio of 0.3. The specific mix proportions of each AARBP paste are shown in Table 1. The precisely weighed brick powder and alkali activator solutions were mixed together in a mixing bowl with high-

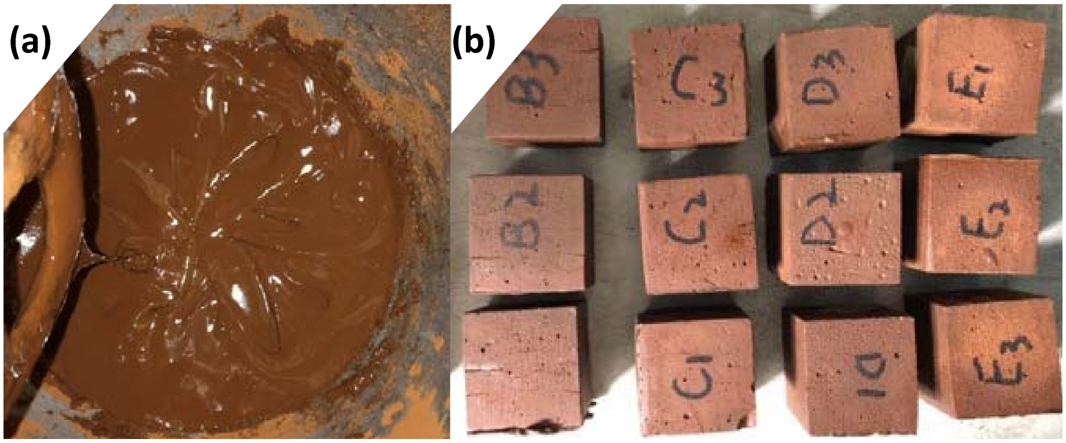

Figure 6: (a) Slurries of the AARBP paste, and (b) the hardened paste cubes.

speed stirrings for 3 min to obtain homogeneous slurries (Fig. 6a). The AARBP paste slurries were then cast into cubic moulds ($40 \times 40 \times 40$ mm^3). High-frequent vibrations were operated to the slurries-filled cubic moulds to remove the air bubbles entrapped in the AARBP pastes. After a surface finishing process, all the open surfaces were covered with a layer of plastic film to avoid the possible drying shrinkage caused by water loss. The moulds were then stored in a sealed chamber with the temperature of 65 ± 2 °C to accelerate the chemical interactions between the brick powder and alkaline activators (Reig et al., 2013; Ulugol et al., 2021a). After 24 hours' primary curing, the paste specimens were demoulded and again sealed with plastic films for further curing in the same chamber. At set ages, all AARBP paste specimens were removed from the curing chamber and cooled in ambient temperature for the designed tests.

Fig. 6b shows a typical picture of the hardened AARBP paste cubes. Apparently, after the alkaline activating processes, the AARBP paste specimens kept the same red color with the sintered clay brick. This aesthetic characteristic of AARBP materials

Table 2: Mix proportions of the non-cement CDW pervious concrete

Sample ID	Brick powder	AS/N ratio	W/B ratio	Aggregate (g)	B/A ratio
CDPC-B/A-0.15	500	6.3	0.3	3333	0.15
CDPC-B/A-0.20	500	6.3	0.3	2500	0.20
CDPC-B/A-0.25	500	6.3	0.3	2000	0.25
CDPC-B/A-0.30	500	6.3	0.3	1667	0.30

may broaden their application scenarios for decorations and repairs other than constructions (Sassoni et al., 2016).

3.2.2. Fabrication of non-cement CDW pervious concrete

The cementitious AARBP material alternative to OPC was used as the binder to fabricate non-cement CDW pervious concretes. The optimum AARBP paste mix (AS/N=6.3) was adopted according to the strength results (section 4.1). The binder-to-aggregate ratio (B/A), as the unique variable to impact the engineering properties of the pervious concrete, was set as 0.15, 0.2, 0.25 and 0.3. The detailed pervious concrete mix proportions are shown in Table 2.

The AARBP paste slurries at the optimum mix were first prepared according to the procedures presented in section 3.2.1. Then the low-quality CDW aggregate (size over 1.18 mm) was poured into the mixing bowl with stirrings at the speed of 120 rpm for 3 min. Due to the relatively low W/B ratio and the discontinuous aggregate grading, the obtained fresh concrete showed almost no fluidity (Fig. 7a). The fresh concrete was

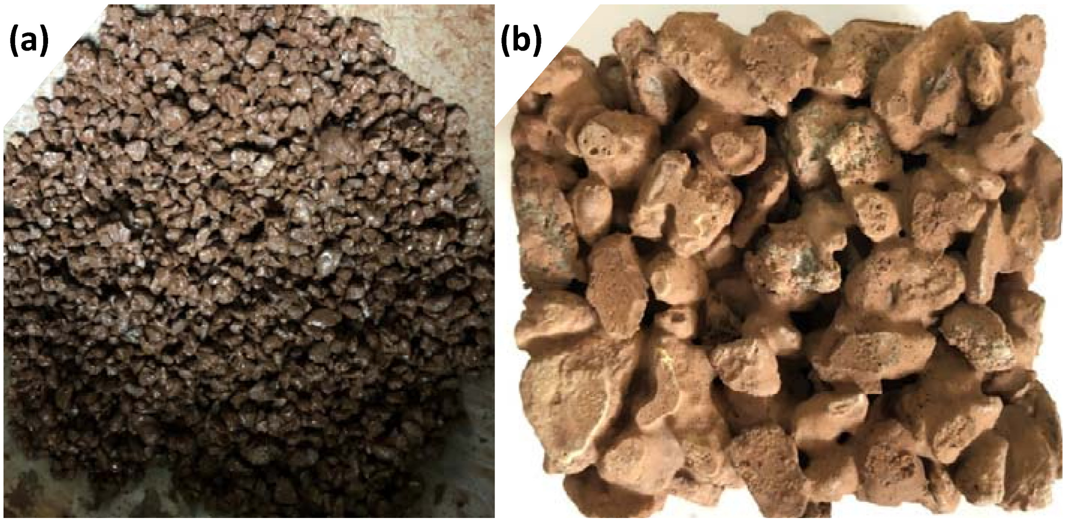

Figure 7: (a) In-situ mixing of pervious concrete, and (b) the hardened cubic specimens.

then cast into cubic moulds ($50 \times 50 \times 50$ mm^3) for strength tests, and cylinder moulds (diameter=63 mm and height=75 mm) for water permeability tests. After the moulds were fully filled with the non-cement CDW concrete, manual press on the specimens was operated to enhance the compactness. No vibrations were used to avoid the possible pore clogging at the bottom of pervious concrete specimens (Cui et al., 2020). The non-cement CDW pervious concrete specimens followed the same curing scheme of the AARBP paste (i.e., sealed curing at 65 ± 2 °C).

Fig. 7b displays a typical picture of a demoulded pervious concrete cube. The specimen surfaces were rough due to the insufficient fillings of the large space between discontinuously graded CDW aggregates. The insufficient space fillings indeed accounted for the high water permeability of pervious concrete in design (AlShareedah and Nassiri, 2021; Xie et al., 2020).

3.3. Methods

3.3.1. Mechanical tests

Compression tests were performed to cubic specimens in an Instron 8802 full functional test machine. The loading speed was maintained at 0.35 kN/s controlled by its electro-hydraulic servo system. As the test proceeded, the forces accumulated, where the maximum values were recorded to calculate compressive strength.

Three independent tests were conducted for each AARBP paste, and six for each CDW pervious concrete due to its large data variance. The statistical results of compression strength for each mix and curing age were analyzed and plotted with the software of Origin (version 9.1).

3.3.2. Water permeability test

Water permability tests for the non-cement CDW pervious concrete were conducted according to a Chinese standard of permeable paving bricks & permeable paving flags (GB/T 25993-2010). A home-made testing setup in a constant-head regime was used to measure the water permeability. As shown in Fig. 8, a cylindrical pervious concrete specimen was first fixed in a plastic tube, where the side surface of the specimen was sealed with an epoxy resin. The tube space above the specimen provided a water reservoir before permeation (named as the top reservoir). The plastic tube, together with the fixed concrete specimen, was put into a bigger plastic bucket that acted as another reservoir (named as the bottom reservoir) to store the permeated water. Two drain pipes were connected to the top and bottom reservoirs respectively to control the

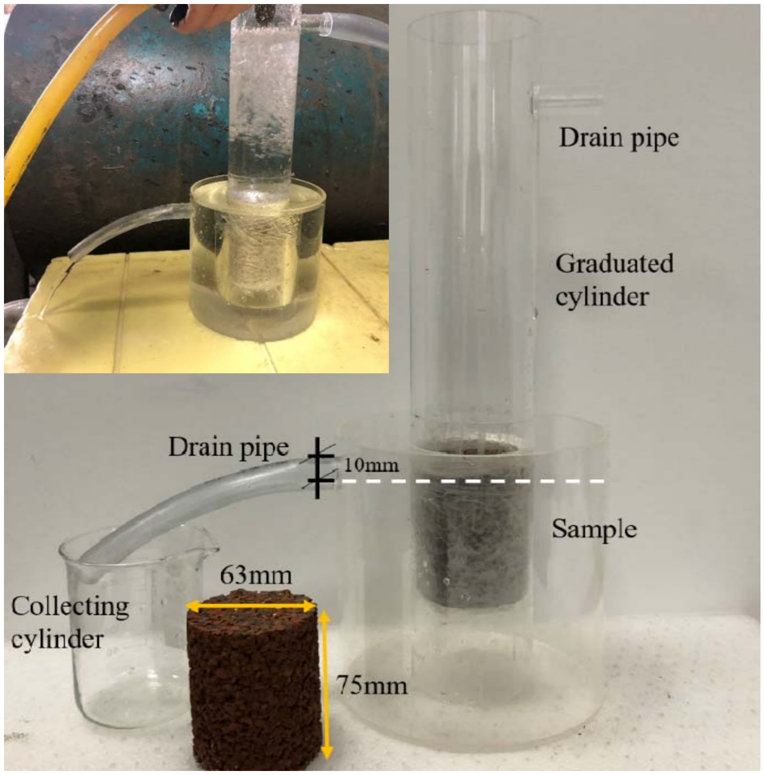

Figure 8: Setup for water permeability test (Inset panel: picture of an in-situ water permeability test).

water head.

During the test, the steady water flows Q in a fixed period t was recorded (see the inset panel of Fig. 8 for a snapshot of in-situ water permeability test), so the water permeability K can be expressed as,

$$K = \frac{QL}{AHt} \tag{1}$$

where L and A are the height and cross sectional area of the specimen, H is the water head. In this work, $L = 7.5$ cm, $A = 31.17$ cm^2 and $H = 18$ cm, so $K = 0.01337Q/t$ (cm/s).

3.3.3. X-ray diffraction

X-ray diffraction (XRD) tests were conducted to characterize the minerals in different AARBP mixes. Each AARBP paste was milled to powder with the 200-mesh passing ratio of 95% for XRD tests. Isopropanol was used as the protecting liquid during milling to avoid the interactions between AARBP hydrates and the air. XRD scans were conducted in a Bruker D8 Advance diffractometer. CuKα radiations with the wavelength of λ=0.15419 nm were applied in the scanning angles between 5 and 90 °with the step length of 0.02 °. A software of MDI Jade 6 was used to identify main mineral phases in the tested samples.

3.3.4. X-ray computed tomography

X-ray computed tomographic (XCT) tests were used to non-destructively measure the macro porosity, pore size/spatial distribution and skeleton of the non-cement CDW pervious concretes, because X-ray attenuation is generally sensitive to material density (Zeng et al., 2019; Brisard et al., 2020). Each concrete cylinder was fixed on the sample frame, and rotated evenly by 360 °in 1800 s during the penetrations of X-ray beams in a device of XTH255/320 LC (Nikon, Japan). The accelerating voltage of 180 kV and the beam current of 160 μA were used. A high-resolution detector (2000 $\times$ 2000 pixels) at the back of the specimen continually recorded the attenuated X-ray beams, and transferred the X-ray attenuation signals to massive transmission X-ray projections at different angles. For each sample, 2500 transmission X-ray projections were recorded and loaded into a CTPro software to generate numerous 8-bit gray images.

A software of VG Studio MAX 3.1 was used for further data processing including region-of-interest (ROI) selection, threshold for phase segmentation, and microstructure reconstruction (Zeng et al., 2020; Qi et al., 2021). The pixel size of the images was 55 μm.

3.3.5. Scanning electron microscopy

Microstructure analysis was performed via a field emission environmental SEM in type of Quanta FEG650. Back-scattered electrons (BSE) mode was applied to obtain high quality BSE images for phase analysis. Small concrete blocks (around 10 mm) including both recycled C&D aggregates and AARBP pastes collected from the central part of pervious concretes were impregnated in cylindrical molds with epoxy resin for sample encasement. After the epoxy resin was hardened, the samples were demoulded and polished in a Buehler semi-automatic polishing machine. Diamond papers in the grade grits of 400, 800, 1200, 2000, and 4000# were used for sample surface polishing with 1 min for each grit. An oven-drying at 40 °Cfor 24 h was performed to remove the capillary water confined in pores of the pervious concrete samples.

During the SEM tests, the accelerating voltage and spot size were set as 20 keV and 5.0 nm, respectively. Images with different magnifications (50× to 1000×) were acquired for the analysis of skeletons, pores, paste microstructure and matrix-aggregate interfaces.

4. Results and discussion

4.1. Optimum AARBP mix

Fig. 9 shows the compressive strengths and densities of the AARBP pastes with 8 different AS/N ratios cured for 7 d and 28 d. Apparently, increasing the curing age systematically raised the compressive strength. Compared with the strength data of the AARBP samples at 7 d (15 to 25 MPa), those at 28 d were greatly increased by between 30% and 93% (22 to 50 MPa) (Fig. 9a). The great strength promotions were caused by the enhanced chemical reactions between the brick powder and alkaline activators under the longer curing periods (Zhang et al., 2021).

Fig. 9a also displays the effects of AS/N ratio on AARBPs' strength. As the AS/N ratio increased from 4 to 9, the compressive strength rose slowly to peak values followed by a rapid fall to nearly constant values. Peak strengths were observed for the mixes with the AS/N ratios of 5.6 and 6.3 (around 25 MPa at 7 d and 50 MPa at 28 d; see the shadowed area shown in Fig. 9a). Too high or too low NaOH content would adversely impact the strength of AARBP, similar trends were reported elsewhere (Tuyan et al., 2018).

Densities of the AARBP pastes at 28 d are illustrated in Fig. 9b. Unlike the rise and fall of compressive strength with AS/N ratio, the samples' density showed an almost monotonously increasing trend from 1600s to 1700s kg/m^3 as AS/N ratio increased. This trend was reasonably caused by the higher density of the activator with higher modulus.

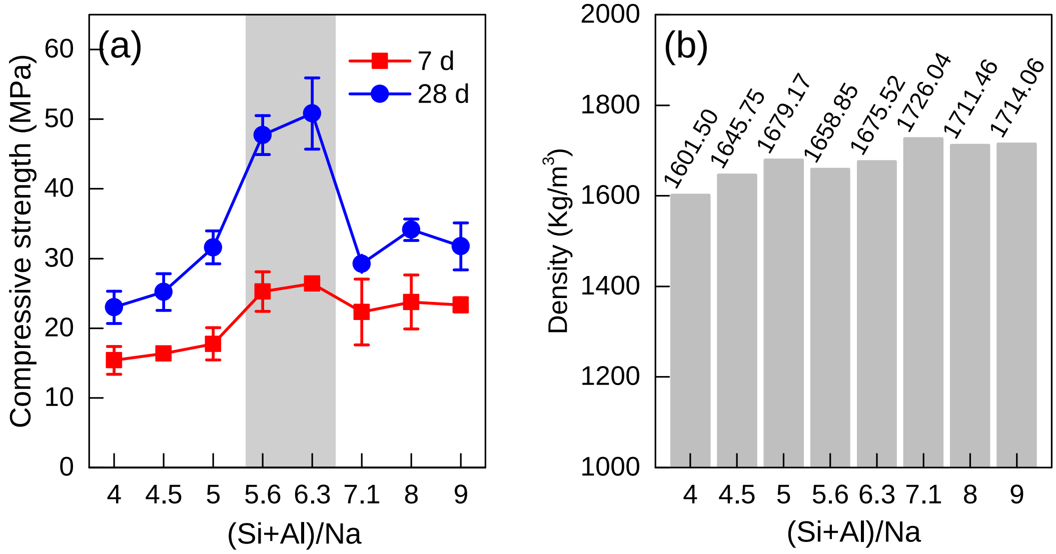

Figure 9: (a) Compressive strength and (b) density of AARBP pastes at different mixes.

It was suspected that AS/N ratios may alter the chemical reaction products, however, the XRD patterns shown in Fig. 10 suggested no significant differences in the hydration products between the AARBP pastes. Characteristic spectra of silica from the sintered clay bricks (quartz) and water glass dominated the XRD patterns with the similar intensities (Fig. 10). Signals of albite ($Na_2O \cdot Al_2O_3 \cdot 6SiO_2$) played the secondly important role on the XRD patterns, implying that the active silica and alumina in brick powder had partially reacted with the alkali activators. However, AS/N ratio seemed to have no impacts on the intensities of albite's XRD spectra (Fig. 10). Considering the similar minerals in the AARBP pastes, the mix of BP-AS/N-6.3 with the highest strength (Fig. 9a) was selected as the basic binder mix for pervious concrete fabrication.

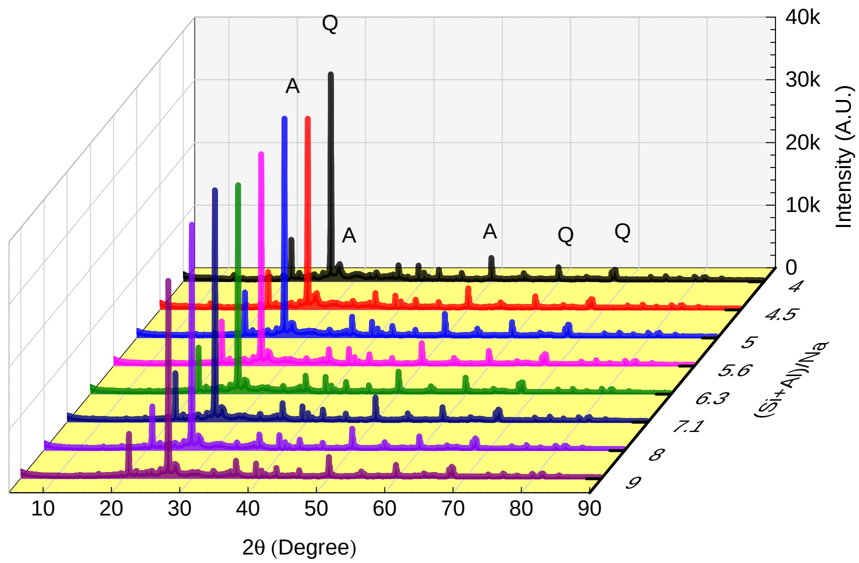

Figure 10: XRD patterns of the alkaline-activated recycled brick powder pastes (Q: Quartz, A: Albite).

4.2. Engineering performances of pervious concrete

Physical and mechanical properties (i.e., compressive strength, density and water permeability coefficient) of the non-cement recycled CDW pervious concrete are illustrated in Figs. 11 and 12. As shown in Fig. 11a, the pervious concrete displayed relatively low compressive strengths (less than 5 MPa for all concrete mixes). At the B/A ratio of 0.15, the concrete blocks only had the strength of 0.6 MPa regardless of curing age, and the density of 1256 kg/m^3 (Fig. 11b), which was even lower than the bulk density of the recycled CDW aggregate (1350 kg/m^3). The low compressive strength and density of CDPC-BA-0.15 were caused by two main reasons: 1), the recycled CDW aggregates were loosely compacted during the concrete fabrication processes because no vibrations were performed to avoid the possible pore clogging; and 2) the limited AARBP paste had poor binding effect on the recycled CDW aggregates (see

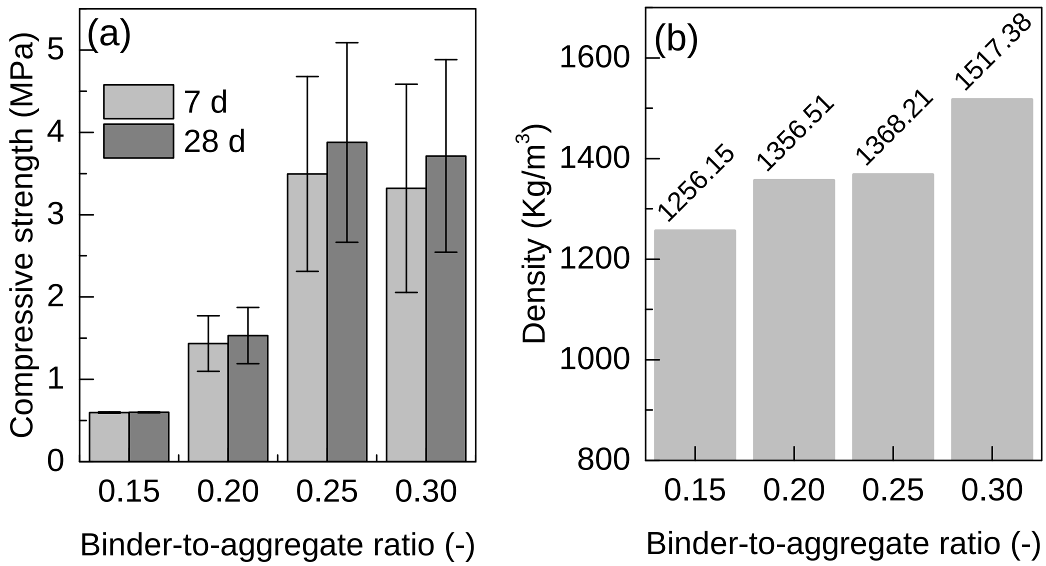

Figure 11: Compressive strength (a) and density (b) of the non-cement pervious concrete with different binder-to-aggregate ratios.

section 4.3.2 for more information).

As the binding phase content (or B/A ratio) increased, the pores were partially filled by the AARBP paste and the bonds between two neighbored CDW aggregates were enhanced, so the compressive strength increased (Fig. 11a). When the B/A ratio was higher than 0.25, the compressive strengths were over 3 MPa. Within the same regime, densities of the non-cement pervious concrete specimens increased with increasing B/A ratio (Fig. 11b). This followed the general concept of pervious concrete design, where increases of the coating paste around aggregates can enhance the mechanical properties of pervious concrete (Shen et al., 2020).

Fig. 12 shows the water permeability coefficients and their relationship with the compressive strengths for the non-cement recycled CDW pervious concrete with different B/A ratios. The water permeability coefficients were greatly higher than the thresholds of pervious concrete pavements and bricks suggested by the code of GB/T 25993-2010 ($K \geq 0.02$ cm/s for level A and ≥ 0.01 cm/s for level B). The high water permeability coefficients were caused by the high contents of connected pores (see section 4.3 for pore structure analysis).

As the B/A ratio increased from 0.15 to 0.3, the water permeability coefficient decreased from 0.48 cm/s to 0.26 cm/s (Fig. 12a). This was certainly induced by the reduction of connected channels for water permeation when more binders were used to fill the gaps between recycled CDW aggregates (see section 4.3.1 for specific evidences). Analysis showed that the water permeability coefficient almost linearly decreased with the increase of compressive strength (Fig. 12b). The results evidenced the opposite roles of the binding phase on the water permeation and strength of pervious concrete (Huang et al., 2021; AlShareedah and Nassiri, 2021).

4.3. Microstructure and mechanisms

Our focuses were then shifted onto the multi-scale structures of the non-cement recycled CDW pervious concrete, which helped explore the pore structure mechanisms of water permeation and strength changes. 3D pore structures resolved by XCT were used to address the connected and isolated pores, while 2D multi-scale measurements by SEM/BSE were applied to address the structure of skeleton, matrix-aggregate ITZ, and AARBP paste.

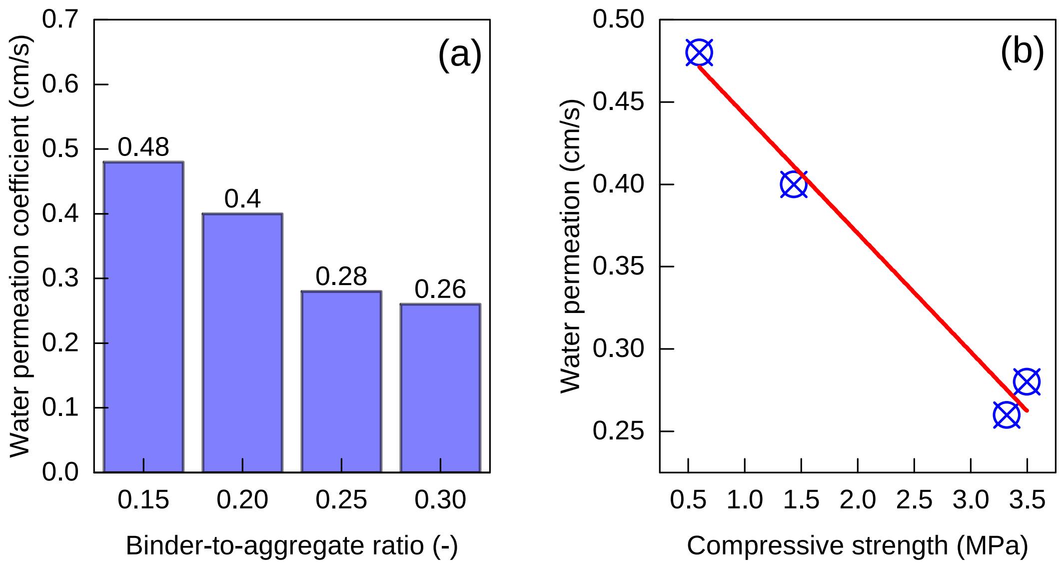

Figure 12: Water permeation coefficient (a) and its relationship with compressive strength (b) of the non-cement recycled C&D wast pervious concrete with different B/A ratios.

4.3.1. Pore structure

Fig. 13 shows 3D structures of the selected pervious concrete cylinders with different B/A ratios, where the connected and isolated pores were separately illustrated in red and blue, respectively. At a first glance, the reconstructed previous concrete cylinders before pore segmentation showed heterogeneous color distributions due to the different attenuation values of different phases (Brisard et al., 2020; Zeng et al., 2019). For the pervious concrete specimens, the lighter color represented the phases with higher X-ray attenuation (e.g., stones and metals), while the darker color denotes the phases with lower X-ray attenuation (e.g., pores and wood pieces); see the bottom half of each overview cylinder shown in Fig. 13. Pore segmentation was then performed on the top half of each cylinder. Clearly, pores were densely distributed in the cylinders, suggesting the highly porous structure of the pervious concrete.

Huge connected pores were identified for each cylinder (middle column of Fig. 13), accounting for the large water permeability coefficients (Fig. 12a). Only small amount of pores were entrapped in the AARBP paste (right column of Fig. 13). Those pores were diagnosed as the isolated or closed pores in the present XCT resolution (55 μm), which would have no significant contribution to water permeation.

The specific cumulative porosity distributions from the XCT data were also analyzed (Fig. 14), as pore size distribution can decisively dominate the water permeability of pervious concrete (Huang et al., 2021). The sharp porosity accumulation at a large size for each pervious concrete was identical to the connected pore shown in Fig. 13. After the pore size decreased by around one order of magnitude, porosity began to rise, suggesting that the isolated pores in different sizes appeared in the AARBP pastes (Fig. 13).

The XCT characterized pore structure was greatly affected by the B/A ratio. First, the B/A ratio impacted the total porosity (Fig. 15). As the designed B/A ratio increased from 0.15 to 0.2, 0.25 and 0.3, the total porosity decreased from 0.43 to 0.33 (by 12%), 0.28 (by 34%) and 0.25 (by 41%), respectively, due to the pore space fillings by the AARBP paste. Consequently, the isolated porosity in the AARBP paste increased from 0.002 (B/A=0.15) to 0.009 (B/A=0.25). The connected porosity showed the similar trend with the total porosity, due to its dominative occupation of the pores (over 96%) (Fig. 15). Second, the B/A ratio also affected the pore size distribution. As demonstrated in Fig. 14, the porosity rising rates increased with the increase of B/A

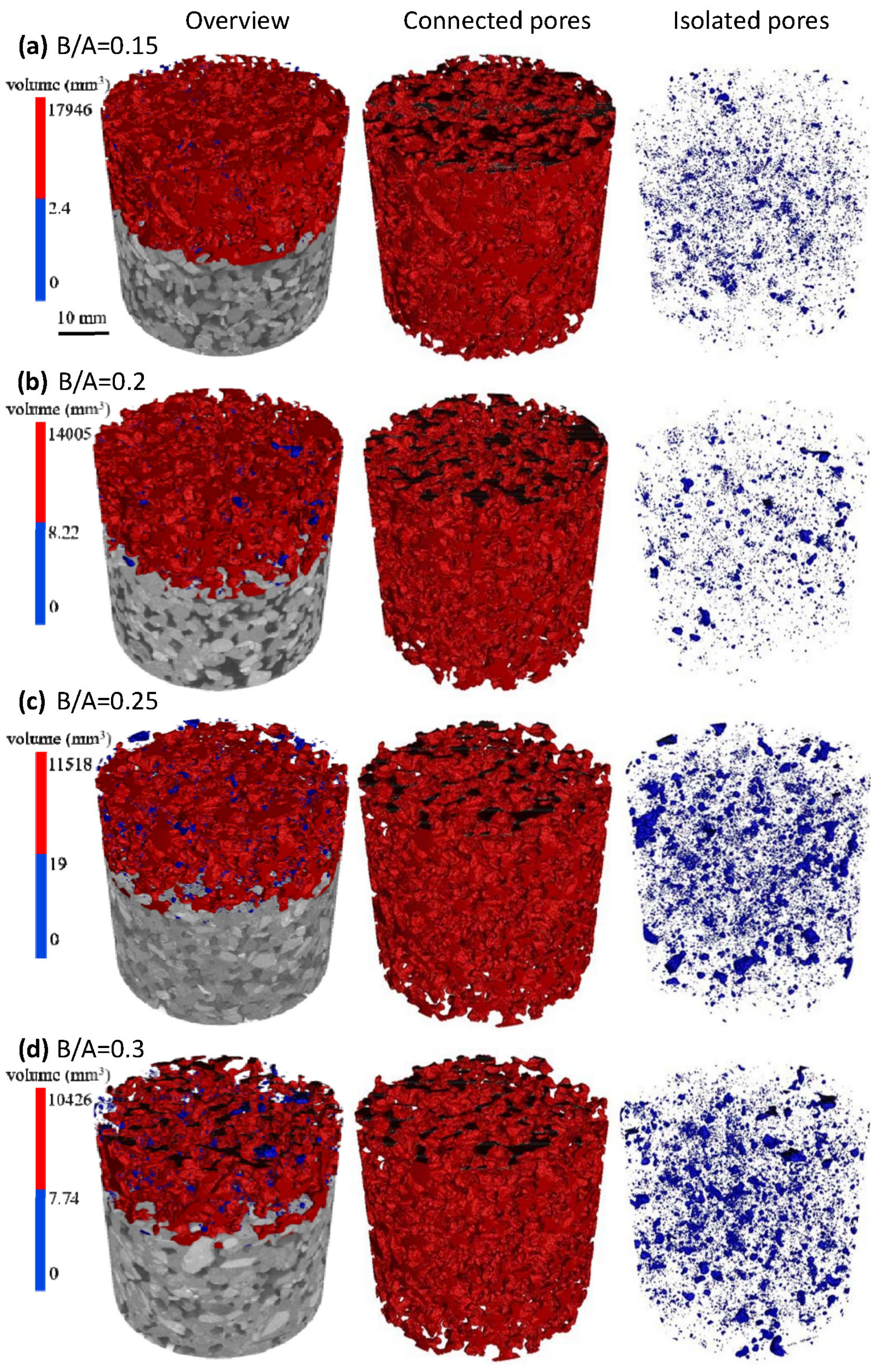

Figure 13: 3D pore structure of pervious concrete cylinders with different B/A ratios: (a) B/A=0.15, (b) B/A=0.20, (c) B/A=0.25, and (d) B/A=0.30 (left: overview of 3D pore structure; middle: connected pores; right: isolated pores).

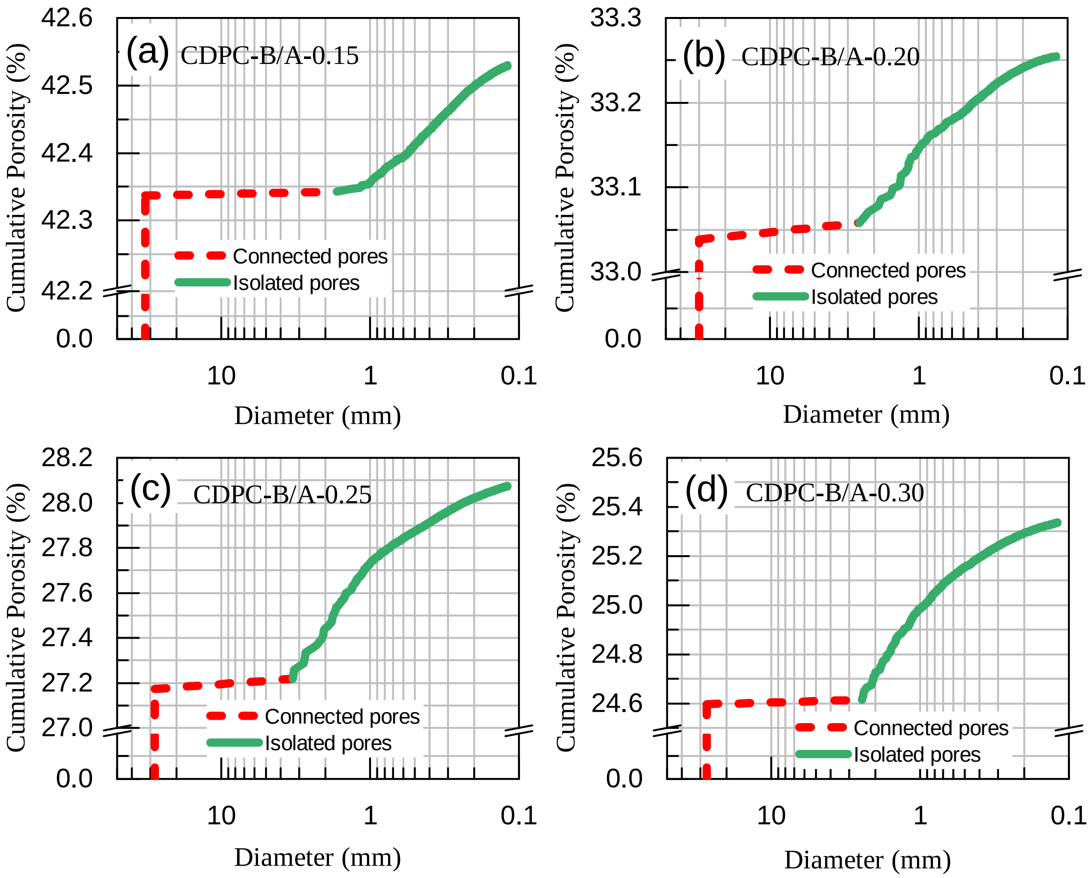

Figure 14: Cumulative connected and isolated pore distributions of (a) CDPC-B/A-0.15, (b) CDPC-B/A-0.20, (c) CDPC-B/A-0.25, and (d) CDPC-B/A-0.30..

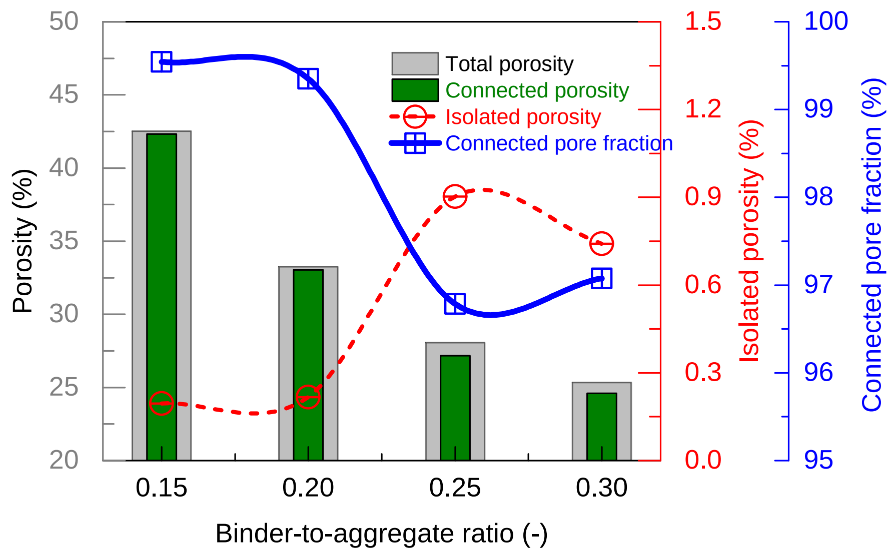

Figure 15: Total, connected and isolated (closed) porosities and the connected pore fraction of the pervious concrete with different binder-to-aggregate ratios.

ratio, and the plot of cumulative porosity versus logarithmic pore diameter progressively changed from linear to non-linear. The accelerated porosity rises were mainly observed at the pore size interval between 1 and 3 mm. Indeed, if those pores were excluded, the porosities with the size below 1 mm showed limited changes with B/A ratio (Fig. 14). The increases of closed macro pores with B/A ratio were directly evidenced by the XCT images (Fig. 13).

4.3.2. Skeleton, paste and ITZ

Skeletons of the pervious concrete samples were observed via BSE images at low magnifications. Figs. 16a-d show the selected 2D BSE images for representative demonstrations. Recycled CDW aggregates were covered with a layer of AARBP paste, and bonded together to form the skeletons, and the rest spaces formed the connected pores

(Fig. 13). For the CDPC-BA-0.15 sample, merely small amount of AARBP paste was attached on the recycled CDW aggregates, forming rough and tortuous skeletons. As shown in Fig. 16a, a needle-like aggregate was insert between two aggregates with the limited bonding areas and paste thickness (around 0.1 mm), leaving the rest spaces to form large, connected pores. This skeleton structure would be certainly not able to sustain high external loads, so the compressive strength was low (Fig. 9). The adverse effect of tortuous skeletons on strength of porous materials was also evidenced from a foamed concrete system (Jin et al., 2021).

As the AARBP paste content increased, the paste layers were thickened and the contacted areas were increased progressively; several recycled CDW aggregates were bonded together to form larger solid clusters (Fig. 16c-d). The average paste thickness was increased to 0.15, 0.22 and 0.36 mm for the samples of CDPC-BA-0.20, CDPC-BA-0.25 and CDPC-BA-0.30, respectively. The increase of skeletons' volume facilitated to build a strengthened structure (AlShareedah and Nassiri, 2021; Shen et al., 2020). As a consequence, both the densities and strengths were substantially raised as the B/A ratio increased (Fig. 9).

It is also interesting to explore the AARBP paste's microstructure and the paste-aggregate ITZ. Fig. 16e shows the local ITZ between AARBP paste and a recycled CDW aggregate for the CDPC-BA-0.25 sample. The relatively large contrast between the paste (darker) and aggregate (brighter) allowed us to easily distinguish between the two phases. No cracks were observed in the ITZ, suggesting the relatively good compatibility and bonds between the paste and recycled aggregate. The rough surfaces of the recycled

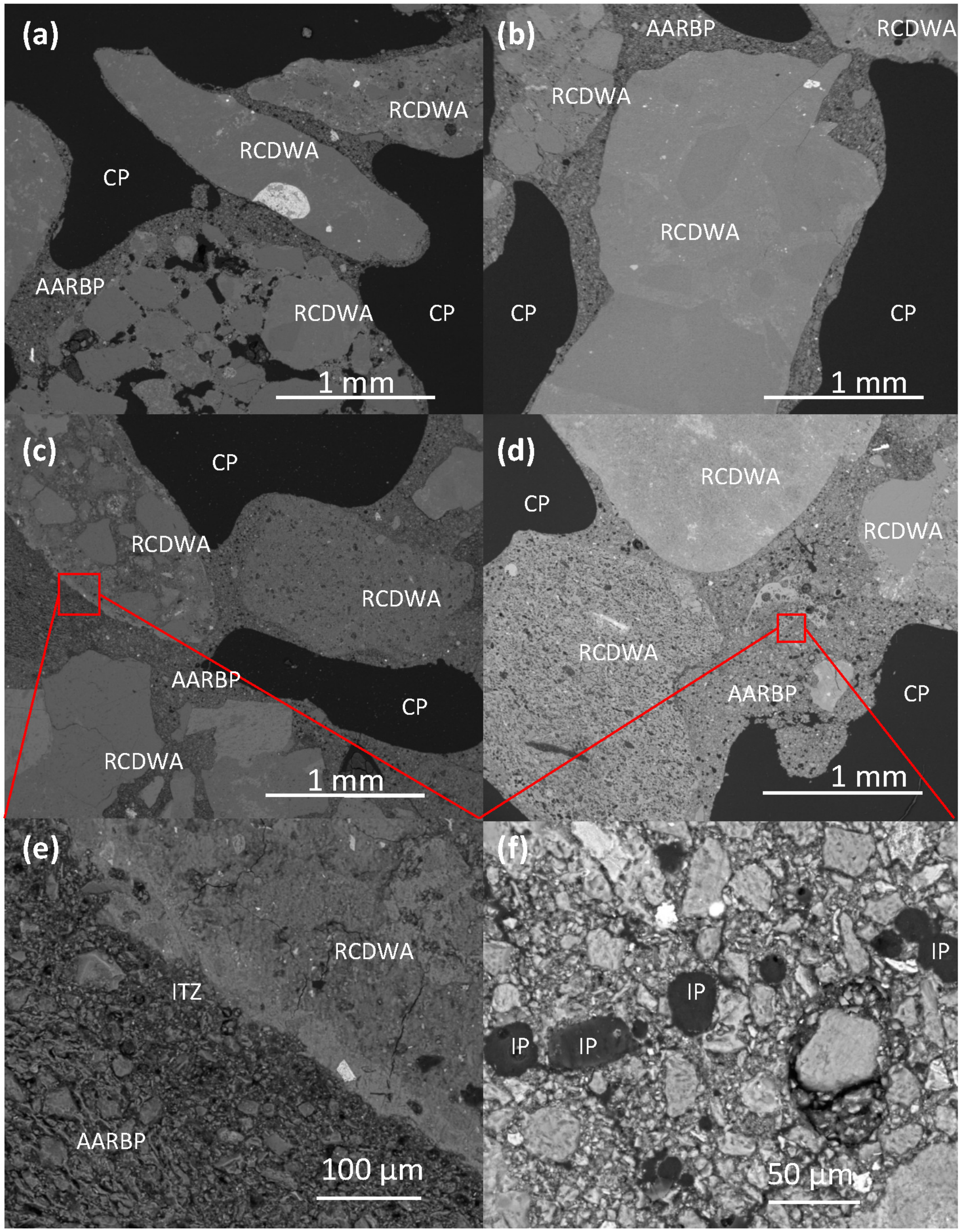

Figure 16: BSE images of (a) CDPC-B/A-0.15, (b) CDPC-B/A-0.2, (c) CDPC-B/A-0.25, (d) CDPC-B/A-0.3, (e) local interfacial area of CDPC-B/A-0.25, and (f) local paste matrix of CDPC-B/A-0.3 (AARBP: alkaline-activated recycled brick paste, RCDWA: recycled CDW aggregate, and P: pore) .

aggregates may account for this observations shown in Fig. 16e. First, cavities on the recycled CDW aggregate surfaces may accommodate fine AARBP particles to enhance the fillings of the ITZ spaces. Second, rough surfaces on the recycled CDW aggregates may provide more sites for the nucleation and growth of the hydration products like CSAH. Both the space filling and nucleation effects may substantially decrease the 'wall effect' that raises the porous structure of ITZ in concrete with natural aggregates (Zhan et al., 2020).

As to the AARBP paste, micro brick particles were compacted together in certain patterns to form the paste matrix that acts as the binding phase to bond the recycled CDW aggregates together. Some large milled brick particles can be clearly observed from the BSE images (Fig. 16f), suggesting the limited reaction extent of the recycled brick powder. However, due to the lack of vibrations, air voids and/or flaws in the thick paste can be not eliminated, so large isolated pores can be seen in Fig. 16f. The entrapped air voids and/or flaws also accounted for the increased pores detected by XCT (Fig. 14d).

4.3.3. Discussion of mechanisms

1, Why is the AARBP strength much higher than that of the non-cement recycled CDW pervious concrete?

The compressive strength of the selected AARBP paste (AS/N=6.3) was as high as 50 MPa (Fig. 9a), higher than that of the non-cement recycled CDW pervious concrete with the same binding material over one order of magnitude (less than 5 MPa; see

Fig. 11a). The most decisive factor is the loose compactness of the CDW aggregates in the pervious concrete system (Pieralisi et al., 2021; Yang et al., 2021). Unlike ordinary concrete that must experience vibrations during specimen casting to enhance the compactness and expel the air voids out of the cement matrix, pervious concrete with severe vibrations was not recommended in order to prevent pore clogging caused by the sinking of paste (Cui et al., 2020). Furthermore, compared with natural aggregates with relatively smooth surfaces, the recycled CDW aggregates have rougher surfaces, leading to the higher frictions between two neighbored aggregates (Li et al., 2019). Consequently, the spatial compactness of rough particles without vibrations would be much looser than that of smooth particles with sufficient vibrations. The attachment of a thin layer of AARBP paste onto the CDW aggregates still can not compensate for the loose compactness, so the density of CDPC-BA-0.15 (Fig. 9b) was even lower than that of the pure CDW aggregates after sufficient vibrations. In the regimes, the non-cement recycled CDW pervious concrete showed relatively low strength.

2, What are the roles that different pores played on the strength and water permeability?

Two different types of pores were diagnosed by XCT according to the pores' connection (Fig. 14), and they would play different roles on water permeability and strength. The connected pores provided open channels for water permeation, while the isolated pores, together with the connected pores, jointly impacted the strength of materials (AlShareedah and Nassiri, 2021; Deo and Neithalath, 2010; Zhang and Wille, 2016). As shown in Fig. 15, all the pervious concrete specimens showed high contents of connected pores, so high water permeabilities were measured (Fig. 12a). As the B/A ratio increased, the skeletons became thicker and the total porosity decreased, so the strength increased (Fig. 9a). However, the method of strength promotion by only increasing paste thickness may be not so effective, as the AARBP pastes were porous (Fig. 13 and 16f). Elimination of the voids and/or flaws in the binding paste may be another way to improve the strength of skeletons, which deserves the further rigorous investigations in the future.

5. Conclusion remarks and perspectives

In this work, low-quality CDW in-situ collected from a local urban-fringe of Hangzhou, China was analyzed; non-cement pervious concrete was fabricated using the recycled CDW aggregates and AARBP paste; and the engineering performances and multi-scale structure of the pervious concrete were systematically investigated. Conclusions can be drawn as follows.

1. The low-quality CDW contained 22.4% dusts and soils with the size below 1.18 mm, and 67.6% macro particles with the size between 1.18 and 10 mm. Concrete (59%), stone (26%), brick (10%) and other solids (5%) in the CDW were recycled as aggregates for the fabrication of pervious concrete.
2. Concept of developing non-cement recycled CDW pervious concrete was proposed. First, sintered clay bricks recycled from the same urban-fringe area were milled to powder and activated by alkaline activators in different AS/N ratios to act as the cementing material. Second, the optimal AARBP paste was mixed with

the recycled CDW aggregates for fabricating non-cement pervious concrete with different B/A ratios.

3. Increasing the curing age systematically promoted the compressive strength of AARBP paste by 30% to 93%. The AARBP paste with the AS/N ratio of 6.3 showed the peak strength of 50 MPa at 28 d. Increasing the AS/N ratio enhanced the AARBP pastes' density, but had no significant impacts on the XRD patterns.
4. The non-cement recycled CDW pervious concrete specimens showed relatively low compressive strength, but high water permeability. Two pore classes (i.e., connected pores and isolated pores) were resolved by XCT. Increasing the B/A ratio decreased the connected porosity, but increased the isolated porosity.
5. The recycled CDW aggregates and the AARBP paste formed tortuous skeletons with limited contribution to strength development. Tight paste-aggregate interactions were observed between the AARBP paste and recycled CDW aggregate. The AARBP paste showed porous microstructure owing to the lack of vibrations during the casting procedures.

Overall, the non-cement recycled CDW pervious concrete fabricated in this work proofed the proposed concept of total recycling of low quality CDW without using external cementing materials. Within the regime, the combined uses of recycled CDW and AARBP paste as the aggregate and binder provide an sustainable solution for the concrete industry. Going beyond this, the ecological benefits of total recycling of CDW (reduction of CO_2 emissions without cement uses) provide promising engineering solutions to the large-scale ongoing buildings and demolitions in China.

Declarations of interest

None.

Acknowledgement

The research is supported by the UCL-ZJU Strategic Partner Funds and Natural Science Foundation of China (No. 51878602). We acknowledge Mr. Yu Peng in Civil Engineering Experiment Center of Zhejiang University for the experiment supports.

References

AlShareedah, O., Nassiri, S., 2021 Pervious concrete mixture optimization, physical, and mechanical properties and pavement design: A review, Journal of Cleaner Production, 288, 125095, https://doi.org/10.1016/j.jclepro.2020.125095.

Amarilla, R. S. D., Ribeiro, R. S., de Avelar Gomes, M. H., Sousa, R. P., Sant'Ana, L. H., Catai, R. E., 2021. Acoustic barrier simulation of construction and demolition waste: A sustainable approach to the control of environmental noise, Applied Acoustics, 182, 108201, https://doi.org/10.1016/j.apacoust.2021.108201.

Bassani, M., Tefa, L., Coppola, B., Palmero, P., 2019a Alkali-activation of aggregate fines from construction and demolition waste: Valorisation in view of road pavement subbase applications, Journal of Cleaner Production, 234, 71-84, https://doi.org/10.1016/j.jclepro.2019.06.207.

Bassani, M., Tefa, L., Russo, A., Palmero, P., 2019b. Alkali-activation of recycled construction and demolition waste aggregate with no added binder, Construction and Building Materials, 205, 398-413, https://doi.org/10.1016/j.conbuildmat.2019.02.031.

Brisard, S., Serdar, M., Monteiro, P. J. M., 2020. Multiscale X-ray tomography of cementitious materials: A review, Cement and Concrete Research, 128, 105824, https://doi.org/10.1016/j.cemconres.2019.105824.

Cai, Y., Lin, X., Yue, W., Zhang, P., 2018. Inexact fuzzy chance-constrained programming for community-scale urban stormwater management, Journal of Cleaner Production, 182, 937-945, https://doi.org/10.1016/j.jclepro.2018.02.009.

Chen, J., Chu, R., Wang, H., Zhang, L., Chen, X., Du, Y., 2019. Alleviating urban heat island effect using high-conductivity permeable concrete pavement, Journal of Cleaner Production, 237, 117722, https://doi.org/10.1016/j.jclepro.2019.117722.

Clark, E., Bleszynski, M., Valdez, F., Kumosa, M., 2020. Recycling carbon and glass fiber polymer matrix composite waste into cementitious materials, Resources, Conservation and Recycling, 155, 104659, https://doi.org/10.1016/j.resconrec.2019.104659.

Collivignarelli, M. C., Abba, A., Miino, M. C., Cillari, G., Ricciardi, P., 2021. A review on alternative binders, admixtures and water for the production of sustainable concrete, Journal of Cleaner Production, 295, 126408, https://doi.org/10.1016/j.jclepro.2021.126408.

Cui, X., Zhang, X., Wang, J., Zhang, J., Qi, H., Li, J., 2020. X-ray CT based clogging analyses of pervious concrete pile by vibrating-sinking tube method, Construction and Building Materials, 262, 120075, https://doi.org/10.1016/j.conbuildmat.2020.120075.

Debnath, B., Sarkar, P. P., 2020. Characterization of pervious concrete using over burnt brick as coarse aggregate, Construction and Building Materials, 242, 118154, https://doi.org/10.1016/j.conbuildmat.2020.118154.

Deo, O., Neithalath, N., 2010. Compressive behavior of pervious concretes and a quantification of the influence of random pore structure features, Materials Science and Engineering: A, 528, 1, 402-412, https://doi.org/10.1016/j.msea.2010.09.024.

Duan, H., Miller, T. R., Liu, G., Tam, V. W. Y., 2019 Construction debris becomes growing concern of growing cities, Waste Management, 83, 1-5. https://doi.org/10.1016/j.wasman.2018.10.044.

Duan, Z., Hou, S., Xiao, J., Singh, A., 2020. Rheological properties of mortar containing recycled powders from construction and demolition wastes, Construction and Building Materials, 237, 117622, https://doi.org/10.1016/j.conbuildmat.2019.117622.

Duan, Z., Singh, A., Xiao, J., Hou, S., 2020. Combined use of recycled powder and recycled coarse aggregate derived from construction and demolition waste in self-compacting concrete, Construction and Building Materials, 254, 119323, https://doi.org/10.1016/j.conbuildmat.2020.119323.

Huang, J., Zhang, Y., Sun, Y., Ren, J., Zhao, Z., Zhang, J., 2021. Evaluation of pore size distribution and permeability reduction behavior in pervious concrete, Construction and Building Materials, 290, 123228, https://doi.org/10.1016/j.conbuildmat.2021.123228.

Ibrahim, H. A., Goh, Y., Ng, Z. A., Yap, S. P., Mo, K. H., Yuen, C. W., Abutaha, F., 2020. Hydraulic and strength characteristics of pervious concrete containing a high volume of construction and demolition waste as aggregates, Construction and Building Materials, 253, 119251, https://doi.org/10.1016/j.conbuildmat.2020.119251.

IEA, 2020. Cement. Paris, https://www.iea.org/reports/cement.

Jin, L., Chen, S., Zhao, Y., Zeng, Q., Huang, Z., Li, M., Shi, Y., 2021. Characterizing the foam-shell microstructure of industrial ultra-light foamed concrete cast under different temperatures, Material Charaction, 173, 110938 https://doi.org/10.1016/j.matchar.2021.110938

Li, L., Liu, W., You, Q., Chen, M., Zeng, Q., 2020a. Waste ceramic powder as a pozzolanic supplementary filler of cement for developing sustainable building materials, Journal of Cleaner Production, 259, 120853, https://doi.org/10.1016/j.jclepro.2020.120853.

Li, L., Liu, W., You, Q., Chen, M., Zeng, Q., Zhou, C., Zhang, M., 2020b. Relationships between microstructure and transport properties in mortar containing recycled ceramic powder, Journal of Cleaner Production, 263, 121384, https://doi.org/10.1016/j.jclepro.2020.121384.

Li, J., Yao, Y., Zuo, J., Li, J., 2020. Key policies to the development of construction and demolition waste recycling industry in China, Waste Management, 108, 137-143, https://doi.org/10.1016/j.wasman.2020.04.016.

Li, L.G., Lin, Z. H., Chen, G. M., Kwan, A. K. H., 2020. Reutilizing clay brick dust as paste substitution to produce environment-friendly durable mortar, Journal of Cleaner Production, 274, 122787, https://doi.org/10.1016/j.jclepro.2020.122787.

Li, X., Dong, M., Jiang, D., Li, S., Shang, Y., 2019. The effect of surface roughness on normal restitution coefficient, adhesion force and friction coefficient of the particle-wall collision, Powder Technology, 362, 17-25, https://doi.org/10.1016/j.powtec.2019.11.120.

Liu, Q., Singh, A., Xiao, J., Li, B., WY Tam, V., 2020. Workability and mechanical properties of mortar containing recycled sand from aerated concrete blocks and sintered clay bricks, Resources, Conservation and Recycling, 157, 104728, https://doi.org/10.1016/j.resconrec.2020.104728.

Liu, Y., Li, T., Yu, L., 2020. Urban heat island mitigation and hydrology performance of innovative permeable pavement: A pilot-scale study, Journal of Cleaner Production, 244, 118938, https://doi.org/10.1016/j.jclepro.2019.118938.

Lu, J., Yan, X., He, P., Poon, C. S., 2019. Sustainable design of pervious concrete using waste glass and recycled concrete aggregate, Journal of Cleaner Production, 234, 1102-1112, https://doi.org/10.1016/j.jclepro.2019.06.260.

Ma, M., Tam, V. W.Y., Le, K. N., Li, W., 2020. Challenges in current construction and demolition waste recycling: A China study, Waste Management, 118, 610-625, https://doi.org/10.1016/j.wasman.2020.09.030.

Meng, T., Hong, Y., Ying, K., Wang, Z., 2021. Comparison of technical properties of cement pastes with different activated recycled powder from construction and demolition waste, Cement and Concrete Composites, 120, 104065, https://doi.org/10.1016/j.cemconcomp.2021.104065.

Olofinnade, O., Ogara, J., 2021 Workability, strength, and microstructure of high strength sustainable concrete incorporating recycled clay brick aggregate and calcined clay, Cleaner Engineering and Technology, 3, 100123, https://doi.org/10.1016/j.clet.2021.100123.

Pieralisi, R., Cavalaro, S.H.P., Aguado, A. 2021. Discrete element modelling of mechanical behaviour of pervious concrete, Cement and Concrete Composites, 119, 104005, https://doi.org/10.1016/j.cemconcomp.2021.104005.

Qi, Y., Liu, K., Peng, Y., Wang, J., Zhou, C., Yan, D., Zeng, Q., 2021. Visualization of mercury percolation in porous hardened cement paste by means of X-ray computed tomography, Cement and Concrete Composites, 122, 104111, https://doi.org/10.1016/j.cemconcomp.2021.104111.

Qin, Y., Pang, X., Tan, K., Bao, T., 2021. Evaluation of pervious concrete performance with pulverized biochar as cement replacement, Cement and Concrete Composites, 119, 104022, https://doi.org/10.1016/j.cemconcomp.2021.104022.

Reig, L., Tashima, M. M., Borrachero, M. V., Monzo, J., Cheeseman, C.R., Paya, J., 2013. Properties and microstructure of alkali-activated red clay brick waste, Construction and Building Materials, 43, 98-106, https://doi.org/10.1016/j.conbuildmat.2013.01.031.

Robalo, K., Costa, H., do Carmo, R., Julio, E., 2021. Experimental development of low cement content and recycled construction and demolition waste aggregates concrete, Construction and Building Materials, 273, 121680, https://doi.org/10.1016/j.conbuildmat.2020.121680.

Robayo, R. A., Mulford, A., Munera, J., M de Gutierrez, R., 2016. Alternative cements based on alkali-activated red clay brick waste, Construction and Building Materials, 128, 163-169, https://doi.org/10.1016/j.conbuildmat.2016.10.023.

Sassoni, E., Pahlavan, P., Franzoni, E., Bignozzi, M. C., 2016. Valorization of brick waste by alkali-activation: A study on the possible use for masonry repointing, Ceramics International, 42 (13), 14685-14694, https://doi.org/10.1016/j.ceramint.2016.06.093.

Shen, W., Liu, Y., Wu, M., Zhang, D., Du, X., Zhao, D., Xu, G., Zhang, B., Xiong, X., 2020. Ecological carbonated steel slag pervious concrete prepared as a key material of sponge city, Journal of Cleaner Production, 256, 120244, https://doi.org/10.1016/j.jclepro.2020.120244.

Shen, W., Wu, M., Zhang, B., Xu, G., Cai, J., Xiong, X., Zhao, D., 2021. Coarse aggregate effectiveness in concrete: Quantitative models study on paste thickness, mortar thickness and compressive strength, Construction and Building Materials, 289, 123171, https://doi.org/10.1016/j.conbuildmat.2021.123171.

Sormunen, P., Karki, T., 2019. Recycled construction and demolition waste as a possible source of materials for composite manufacturing, Journal of Building Engineering, 24, 100742, https://doi.org/10.1016/j.jobe.2019.100742.

Sun, C., Chen, L., Xiao, J., Singh, A., Zeng, J., 2021. Compound utilization of construction and industrial waste as cementitious recycled powder in mortar, Resources, Conservation and Recycling, 170, 105561, https://doi.org/10.1016/j.resconrec.2021.105561.

Tan, K., Qin, Y., Du, T., Li, L., Zhang, L., Wang, J. 2021. Biochar from waste biomass as hygroscopic filler for pervious concrete to improve evaporative cooling performance, Construction and Building Materials, 287, 123078, https://doi.org/10.1016/j.conbuildmat.2021.123078.

Tang, Q., Ma, Z., Wu, H., Wang, W., 2020. The utilization of eco-friendly recycled powder from concrete and brick waste in new concrete: A critical review, Cement and Concrete Composites, 114, 103807, https://doi.org/10.1016/j.cemconcomp.2020.103807.

Tefa, L., Bassani, M., Coppola, B., Palmero, P., 2021. Strength development and environmental assessment of alkali-activated construction and demolition waste fines as stabilizer for recycled road materials, Construction and Building Materials, 289, 123017, https://doi.org/10.1016/j.conbuildmat.2021.123017.

Tuyan, M., Andic-cakir, O., Ramyar, K., 2018. Effect of alkali activator concentration and curing condition on strength and microstructure of waste clay brick powder-based geopolymer, Composites Part B: Engineering, 135, 242-252, https://doi.org/10.1016/j.compositesb.2017.10.013.

Ulugol, H., Kul, A., Yildirim, G., Sahmaran, M., Aldemir, A., Figueira, D., Ashour, A., 2021. Mechanical and microstructural characterization of geopolymers from assorted construction and demolition waste-based masonry and glass, Journal of Cleaner Production, 280, Part 1, 124358, https://doi.org/10.1016/j.jclepro.2020.124358.

Ulugol, H., Gunal, M. F., Yaman, I. O., Yildirim, G., Sahmaran, M., 2021. Effects of self-healing on the microstructure, transport, and electrical properties of 100% construction- and demolition-waste-based geopolymer composites, Cement and Concrete Composites, 121, 104081, https://doi.org/10.1016/j.cemconcomp.2021.104081.

Vieira, G. L., Schiavon, J. Z., Borges, P. M., da Silva, S. R., de Oliveira Andrade, J. J., 2020. Influence of recycled aggregate replacement and fly ash content in performance of pervious concrete mixtures, Journal of Cleaner Production, 271, 122665, https://doi.org/10.1016/j.jclepro.2020.122665.

Xiao, J., Ma, Z., Sui, T., Akbarnezhad, A., Duan, Z., 2018. Mechanical properties of concrete mixed with recycled powder produced from construction and demolition waste, Journal of Cleaner Production, 188, 720-731, https://doi.org/10.1016/j.jclepro.2018.03.277.

Xie, X., Zhang, T., Wang, C., Yang, Y., Bogush, A., Khayrulina, E., Huang, Z., Wei, J., Yu, Q., 2020. Mixture proportion design of pervious concrete based on the relationships between fundamental properties and skeleton structures, Cement and Concrete Composites, 113, 103693, https://doi.org/10.1016/j.cemconcomp.2020.103693.

Yan, D., Chen, S., Zeng, Q., Xu, S., Li, H., 2016. Correlating the elastic properties of metakaolin-based geopolymer with its composition, Materials & Design, 95, 306-318, https://doi.org/10.1016/j.matdes.2016.01.107.

Yang, L., Kou, S., Song, X., Lu, M., Wang, Q., 2021. Analysis of properties of pervious concrete prepared with difference paste-coated recycled aggregate, Construction and Building Materials, 269, 121244, https://doi.org/10.1016/j.conbuildmat.2020.121244.

Yazdani, M., Kabirifar, K., Frimpong, B. E., Shariati, M., Mirmozaffari, M., Boskabadi, A., 2021. Improving construction and demolition waste collection service in an urban area using a simheuristic approach: A case study in Sydney, Australia, Journal of Cleaner Production, 280, Part 1, 124138, https://doi.org/10.1016/j.jclepro.2020.124138.

Zeng, Q., Wang, X., Yang, P., Wang, J., Zhou, C., 2019. Tracing mercury entrapment in porous cement paste after mercury intrusion test by X-ray computed tomography and implications for pore structure characterization, Materials Characterization, 151, 203-215, https://doi.org/10.1016/j.matchar.2019.02.014.

Zeng, Q., Chen, S., Yang, P., Peng, Y., Wang, J., Zhou, C., Wang, Z., Yan, D., 2020. Reassessment of mercury intrusion porosimetry for characterizing the pore structure of cement-based porous materials by monitoring the mercury entrapments with X-ray computed tomography, Cement and Concrete Composites, 113, 103726, https://doi.org/10.1016/j.cemconcomp.2020.103726.

Zhan, B. J., Xuan, D. X., Poon, C. S., Scrivener, K. L., 2020. Characterization of interfacial transition zone in concrete prepared with carbonated modeled recycled concrete aggregates, Cement and Concrete Research, 136, 106175, https://doi.org/10.1016/j.cemconres.2020.106175.

Zhang, J., Zhang, A., Huang, C., Yu, H., Zhou, C., 2021. Characterising the resilient behaviour of pavement subgrade with construction and demolition waste under Freeze?Thaw cycles, Journal of Cleaner Production, 300, 126702, https://doi.org/10.1016/j.jclepro.2021.126702.

Zhong, R., Wille, K., Linking pore system characteristics to the compressive behavior of pervious concrete, Cement and Concrete Composites, 70, 130-138, https://doi.org/10.1016/j.cemconcomp.2016.03.016.

Zhang, Z., Wong, Y. C., Arulrajah, A., 2021. Feasibility of producing non-fired compressed masonry units from brick clay mill residues by alkali activation, Journal of Cleaner Production, 306, 126916, https://doi.org/10.1016/j.jclepro.2021.126916.

Zhou, B., Zhang, J., Pei, J., Li, R., Zhang, Z., 2021. Design and evaluation of high?luminance porous asphalt mixtures based on wasted glass for sponge city, Construction and Building Materials, 273, 121696, https://doi.org/10.1016/j.conbuildmat.2020.121696.